

ADVANCED POWDER TECHNOLOGY

PUBLISHER: ELSEVIER

Editor-in-Chief

Professor Dr. Shuji Matsusaka, Department of Chemical Engineering, Kyoto University, Kyoto, Japan.

ISSN: 0921-8831

IMPACT FACTOR= 2.478

Accepted October 21st 2016

MHD convective heat transfer of nanofluids through a flexible tube with buoyancy: A study of nano-particle shape effects

¹Noreen Sher Akbar, ²Dharmendra Tripathi and ³O. Anwar Bég

¹*DBS&H CEME National University of Sciences and Technology, Islamabad, Pakistan*

²*Department of Mechanical Engineering, Manipal University Jaipur, Rajasthan-303007, India.*

³*Fluid Mechanics, Bio-Propulsion and Nanosystems, Aeronautical/Mechanical Engineering, University of Salford, Newton Building, The Crescent, Salford, Manchester, M5 4WT, UK*

ABSTRACT:

This paper presents an analytical study of magnetohydrodynamics and convective heat transfer of nanofluids synthesized by three different shaped (brick, platelet and cylinder) silver (Ag) nanoparticles in water. A two-phase nanoscale formulation is adopted which is more appropriate for biophysical systems. The flow is induced by metachronal beating of cilia and the flow geometry is considered as a cylindrical tube. The analysis is carried out under the low Reynolds number and long wavelength approximations and the fluid and cilia dynamics is of the creeping type. A Lorentzian magnetic body force model is employed and magnetic induction effects are neglected. Solutions to the transformed boundary value problem are obtained via numerical integration. The influence of cilia length parameter, Hartmann (magnetic) number, heat absorption parameter, Grashof number (free convection), solid nanoparticle volume fraction, and cilia eccentricity parameter on the flow and heat transfer characteristics (including effective thermal conductivity of the nanofluid) are examined in detail. Furthermore a comparative study for different nanoparticle geometries (i.e. bricks, platelets and cylinders) is conducted. The computations show that pressure increases with enhancing the heat absorption, buoyancy force (i.e. Grashof number) and nanoparticle fraction however it reduces with increasing the magnetic field. The computations also reveal that pressure enhancement is a maximum for the platelet nano-particle case compared with the brick and cylinder nanoparticle cases. Furthermore the quantity of trapped streamlines for cylinder type nanoparticles exceeds substantially that computed for brick and platelet nanoparticles, whereas the bolus magnitude (trapped zone) for brick nanoparticles is demonstrably greater than that obtained for cylinder and platelet nanoparticles. The present model is applicable in biological and biomimetic transport phenomena exploiting magnetic nanofluids and ciliated inner tube surfaces.

Keywords: Magnetohydrodynamics; heat and mass transfer; cilia induced flow; silver-water nanofluids; bio-propulsion; nanoparticle fraction.

*Corresponding author- Email: noreen.sher@ceme.nust.edu.pk, noreensher@yahoo.com

1. INTRODUCTION

Magnetohydrodynamic (MHD) convective heat and mass transfer of metallic-water nanofluids induced by cilia motion has garnered some interest owing to emerging applications in biomedical engineering, biomimetic thermal design [1] etc. MHD is the study of magnetic properties of electrically-conducting fluids including salt water, plasma etc. It is simulated using the equations of fluid dynamics coupled with Maxwell's electromagnetic field equations. Convective heat transfer is process of heat transport from one place to another place by movement of fluids which works on principle of energy conservation. Modern nanotechnology fluid systems utilize *nanofluids* which are synthesized by the suspension of nanoparticles of size 1-50nm within a base fluid e.g. water. The term “nanofluids” was first proposed by Choi [2]. The study of nanofluids is a major advance in thermal engineering since heat transfer performance has been proven to be substantially better with nanofluids than pure liquids. Nanofluids exhibit superior properties compared to conventional heat transfer fluids, as well as fluids containing nano-sized metallic particles. Since the radius of nanoparticles is very small then the relative surface area of nanoparticles is much larger than conventional particles. As a result the stability of suspensions of nanoparticles is comparatively better. Good summaries of recent developments in research on the heat transfer characteristics of nanofluids include the reviews by Das *et al.* [3], Wen *et al.* [4], Trisaksri and Wongwises [5] and Wang and Majumdar [6]. These have identified numerous applications of nanofluids in areas ranging from solar collector design to anti-bacterial medical systems. These reviews have also emphasized that suspended nanoparticles remarkably increase the forced convective heat transfer performance of the base fluid and furthermore that at the same Reynolds number heat transfer in nanofluids increases with the particle volume fraction. Many studies addressing magnetohydrodynamic nanofluid flows have appeared employing a diverse range of nano-particle models and also different numerical and analytical methods to solve the conservation equations. These investigations involve models which amalgamate the physics of MHD and energy, mass, momentum conservation principles. Uddin *et al.* [7] used a finite element algorithm to investigate magnetic field effects on radiative conducting nanofluid transport from a stretching sheet with hydrodynamic and thermal slip effects. Sheikholeslami *et al.* [8] used a Lattice Boltzmann method and KKL (Koo–Kleinstreuer–Li) correlation to investigate nanofluid flow and heat transfer in an enclosure heated from below. They observed

that heat transfer is elevated with greater magnetic (Hartmann) number and heat source length whereas it is reduced with greater Rayleigh number. Bég *et al.* [9] deployed a homotopy analysis method to compute the influence of porous media drag on nanofluid boundary layer flow from a sphere. Makinde *et al.* [10] used the 4th order Runge-Kutta method to analyze free convection effects on magnetized stagnation point flow of nanofluids from both shrinking and stretching sheets. Turkyilmazoglu *et al.* [11] obtained closed-form solutions for magnetic nanofluid boundary layer slip flow from an extending/contracting sheet, observing that a unique solution exists for the stretching sheet scenario whereas multiple solutions are observed for the shrinking sheet case. Akbar *et al.* [12] investigated analytically the influence of different nanoparticle geometries (brick, platelet and cylindrical) on heat transfer characteristics in magnetic peristaltic nanofluid pumping. They observed that increasing Hartmann number (magnetic body force) accelerates the flow for the case of platelet nanoparticles but induces deceleration for brick nanoparticles. They further identified that thermal conductivity is a maximum for brick-shaped nanoparticles. Bég *et al.* [13] employed Maple software and finite difference codes to study the influence of wall temperature variation and surface tension (Marangoni effect) on hydromagnetic nanofluid boundary layer flow. Fullstone *et al.* [14] used a two-phase approach to simulate agent based effects in nanoparticle transport in blood flow. Kahan and Khan [15] studied power-law index and mass boundary condition effects on hydromagnetic non-Newtonian nanofluid transport. Recent experimental work by Bao *et al.* [16] has further established the importance of magnetic nanofluids in medical engineering including new areas such as lithography, magnetic particle imaging, magnetic-assisted pharmacokinetics and positive contrast agents of potential benefit in magnetic resonance imaging.

Biological fluid dynamics has also continued to embrace new frontiers of emerging technologies. Medical applications provide an excellent forum for combining many areas of science and engineering simulation to develop multi-faceted solutions for complex phenomena. Mathematical models are therefore increasingly merging the concepts of engineering mechanics, biology and chemistry with a diverse array of computational methods. Surface science in medicine has exposed engineers to the mechanism of cilia movement. Cilia are hair-like (nano size) structures that can beat and generate metachronal waves in synchrony causing the movement of unicellular paramecium. There two types of cilia - motile and non-motile (or

primary cilia). Non-motile or primary cilia are found in nearly every cell in all mammals and do not beat. They are found in human sensory organs such as the eye and the nose. Motile cilia are found on the surface of cells and they beat in a rhythmic manner i.e. they exhibit a continuous pattern of contraction and relaxation which is very similar to the pattern like peristaltic movement. They are found in the lining of the trachea (windpipe), where they sweep mucus and dirt out of the lungs and the beating of cilia in the fallopian tubes of female mammals moves the ovum from the ovary to the uterus. Considering this oscillating movement as being similar to a metachronal wave in living systems, various researchers have developed mathematical models to describe the fluid mechanics of this phenomenon. Sleight [17] discussed the propulsion of cilia as metachronic wave. Sleight and Aiello [18] further reported on the movement of water by cilia. Miller [19] investigated the movement of Newtonian fluids sustained by mechanical cilia. Blake [20] implemented a spherical envelope approach for simulating ciliary propulsion. Blake [21] further reported interesting mathematical results for cilia-induced Stokes flows in tubules. Cilia propulsion has also attracted some attention in recent years, largely motivated by biomimetic systems and new trends in nanotechnology. Khaderi *et al.* [22] studied the performance of magnetically-driven artificial cilia for lab-on-a-chip applications. Dauplain *et al.* [23] discussed the hydrodynamics of ciliary propulsion. Khaderi *et al.* [24] further examined metachronal motion of symmetrically beating cilia. Khaderi and Onck [25] developed a numerical model to analysis the interaction of magnetic artificial cilia with surrounding fluids in three-dimensional flow systems, motivated by pharma-nano-robotics. Kotsis *et al.* [26] reviewed developments in cilia flow sensors in treatment of polycystic kidney diseases. Brown and Bitman [27] explored the roles of cilia in human health and diseases. Akbar and Butt [28] developed a mathematical model for heat transfer in viscoelastic fluid flow induced cilia movement. Akbar and Khan [29] studied the metachronal beating of cilia in magnetized viscoplastic fluids using a modified Casson non-Newtonian model. Akbar and Khan [30] further explored heat transfer in bi-viscous fluids induced by ciliary motion. Nadeem and Sadaf [31] presented analytical solutions for copper-nano-particle-blood flow under metachronal wave of cilia motion in a curved channel.

The above studies however did not explore the influence of *nano-particle geometry* on transport phenomena in cilia-induced propulsion. Motivated by novel developments in magnetic-assisted gastric treatments [32] and biomimetic cilia magnetic propulsion [33, 34], in the present

article we present a new mathematical model to study the magnetohydrodynamic flow and convective heat transfer effects on cilia movement of Ag-water nanofluids through a cylindrical vessel. A Lorentzian magnetic force model is considered in the present study and magnetic induction effects are neglected. Analytical solutions for velocity, temperature and pressure are obtained under the assumption of low Reynolds number and long wavelength approximation i.e. lubrication theory. The influence of three different nano-particle geometries, thermal buoyancy and heat source on flow and heat transfer characteristics for silver-water nanofluid are investigated. Furthermore geometric effects of the ciliary movement are also studied with the help of graphical and numerical results. The present analysis is relevant to further elucidating transport phenomena in nanofluid biomimetic cilia-actuated magnetohydrodynamic propulsion systems.

2. MATHEMATICAL FORMULATION

Consider an axisymmetric flow of silver-water suspended nanofluids through a vertical circular deformable tube (Fig. 1). A two-phase nanoscale formulation is deployed which is more appropriate for biophysical transport, as elaborated in Bég *et al.* [13] and Fullstone *et al.* [14]. This methodology more realistically described medical (blood) flows compared with the single-phase formulation in nanofluids since it relates to fluid-particle systems more closely.

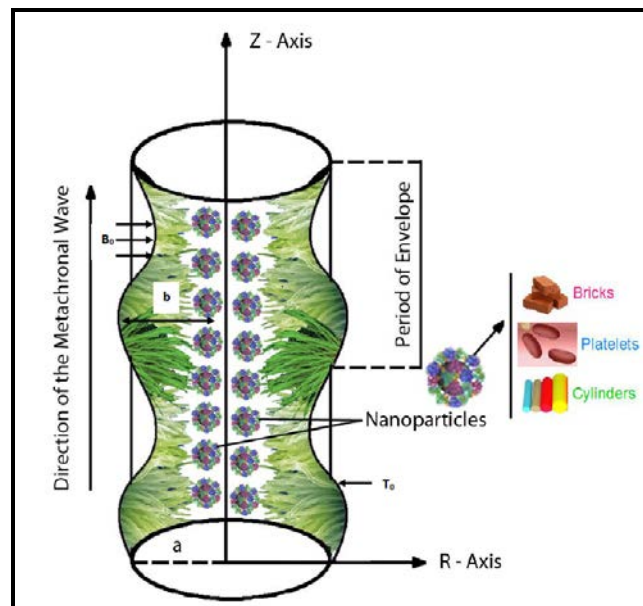


Fig.1. Geometry of the problem.

The inner surface of the circular tube is ciliated with metachronal waves and the flow occurs due to collective beating of the cilia. The nanofluid suspension is electrically-conducting and thermal buoyancy (free convection) effects are present. Both magnetohydrodynamics and convective heat transfer analysis for nanofluids are therefore taken into account. For magnetohydrodynamics, there is an extra term due to the MHD body force, $J \times B$, which is required in the momentum equations, where J is the electric current density and B the magnetic flux. J is defined in the generalized Ohm's law as follows:

$$J = \sigma (E + V \times B), \quad (1)$$

The Maxwell electromagnetic field equations in vector form are:

$$\text{div } D = \rho_e, \text{ div } H = 0, \text{ curl } E = -\frac{\partial B}{\partial t}, \text{ curl } H = J + \frac{\partial D}{\partial t}, \quad (2)$$

where σ is the electrical conductivity of nanofluid, E the electric field, D the electric displacement field, ρ_e the free electron charge density and H the magnetic field strength. Any material can be treated as linear, as long as the electric and magnetic fields are not extremely strong. In a linear medium, the microscopic field strengths D and H are related with the field strengths E and B via material-dependent constants, viz., the electric and magnetic permeabilities, ε and μ_m respectively, and are given by:

$$D = \varepsilon E, \quad B = \mu_m H. \quad (3)$$

For a linear medium, Maxwell's equations with no charge density and electric displacement reduce to the following forms:

$$\text{div } E = 0, \quad \text{div } B = 0, \quad \text{curl } E = -\frac{\partial B}{\partial t}, \quad \text{curl } B = \mu_m J. \quad (4)$$

Introducing the appropriate magnetic field terms (which are linear functions of velocity), the governing equations of motion (mass, momentum and energy conservation) for electrically-conducting nanofluids in a cylindrical coordinate system (\bar{r}, \bar{z}) may be presented as:

$$\frac{1}{\bar{r}} \frac{\partial(\bar{r}\bar{u})}{\partial \bar{r}} + \frac{\partial \bar{w}}{\partial \bar{z}} = 0, \quad (5)$$

$$\rho_{nf} \left[\bar{u} \frac{\partial \bar{u}}{\partial \bar{r}} + \bar{w} \frac{\partial \bar{u}}{\partial \bar{z}} \right] = -\frac{\partial \bar{P}}{\partial \bar{r}} + \mu_{nf} \frac{\partial}{\partial \bar{r}} \left[2 \frac{\partial \bar{u}}{\partial \bar{r}} \right] + \mu_{nf} \frac{2}{\bar{r}} \left(\frac{\partial \bar{u}}{\partial \bar{r}} - \frac{\bar{u}}{\bar{r}} \right) + \mu_{nf} \frac{\partial}{\partial \bar{z}} \left[\left(\frac{\partial \bar{u}}{\partial \bar{r}} + \frac{\partial \bar{w}}{\partial \bar{z}} \right) \right], \quad (6)$$

$$\rho_{nf} \left[\bar{u} \frac{\partial \bar{w}}{\partial \bar{r}} + \bar{w} \frac{\partial \bar{w}}{\partial \bar{z}} \right] = -\frac{\partial \bar{P}}{\partial \bar{z}} + \frac{\mu_{nf}}{\rho_{nf}} \frac{\partial}{\partial \bar{z}} \left[2 \frac{\partial \bar{w}}{\partial \bar{z}} \right] + \mu_{nf} \frac{1}{\bar{r}} \frac{\partial}{\partial \bar{r}} \left[\bar{r} \left(\frac{\partial \bar{u}}{\partial \bar{z}} + \frac{\partial \bar{w}}{\partial \bar{r}} \right) \right] - \sigma B_o^2 (\bar{w} + c) + \rho_{nf} g \alpha (\bar{T} - T_0), \quad (7)$$

$$(\rho_{cp})_{nf} \left(\bar{u} \frac{\partial \bar{T}}{\partial \bar{r}} + \bar{w} \frac{\partial \bar{T}}{\partial \bar{z}} \right) = k_{nf} \left[\frac{\partial^2 \bar{T}}{\partial \bar{r}^2} + \frac{1}{\bar{r}} \frac{\partial \bar{T}}{\partial \bar{r}} + \frac{\partial^2 \bar{T}}{\partial \bar{z}^2} \right] + Q_0. \quad (8)$$

where \bar{r} and \bar{z} are the radial and axial coordinates (i.e. \bar{z} is taken as the center line of the tube and \bar{r} transverse to it), \bar{u} and \bar{w} are the velocity components in the \bar{r} and \bar{z} directions respectively, c is wave velocity, \bar{T} is the local temperature of the fluid. Further, ρ_{nf} is the effective density, μ_{nf} is the effective dynamic viscosity, $(\rho c_p)_{nf}$ is the heat capacitance, α_{nf} is the effective thermal diffusivity, and k_{nf} is the effective thermal conductivity of the nanofluid, which are defined (see Nadeem and Sadaf [31]) as:

$$\left. \begin{aligned} \rho_{nf} &= (1-\phi)\rho_f + \phi\rho_f, \quad \mu_{nf} = \frac{\mu_f}{(1-\phi)^{2.5}}, \\ \alpha_{nf} &= \frac{k_{nf}}{(\rho c_p)_{nf}}, \quad (\rho c_p)_{nf} = (1-\phi)(\rho c_p)_f + \phi(\rho c_p)_s, \\ k_{nf} &= k_f \left(\frac{k_s + (m+1)k_f - (m+1)(k_f - k_s)\phi}{k_s + (m+1)k_f + \phi(k_f - k_s)} \right). \end{aligned} \right\} \quad (9)$$

Here ϕ is the solid nanoparticle volume fraction, k_s and k_f are the thermal conductivities of the particle material and the base fluid, and m is the geometrical shape factor. Values of shape factor for nanoparticles with brick, platelet and cylinder geometries are respectively 3.7, 5.7 and 4.9. Hamilton and Crosser [A] developed a robust approach to simulate irregular particle geometries by introducing a shape factor. According to this model, when the thermal conductivity of the nanoparticles is 100 times larger than that of the base fluid, the thermal conductivity can be expressed as given in eqn. (9). The thermal conductivity and viscosity of various shapes of alumina nanoparticles in a fluid were investigated by Timofeeva *et al.* [B]. They analyzed experimental data accompanied by theoretical modelling for different shapes of nanoparticles, which are given in **Table 1**.

Introducing the following non-dimensional variables:

$$\begin{aligned}
r &= \frac{\bar{r}}{a}, \quad z = \frac{\bar{z}}{\lambda}, \quad w = \frac{\bar{w}}{c}, \quad u = \frac{\lambda \bar{u}}{ac}, \quad p = \frac{a^2 \bar{p}}{c \lambda \mu_f}, \quad \delta = \frac{a}{\lambda}, \quad \theta = \frac{(\bar{T} - \bar{T}_0)}{\bar{T}_0}, \quad t = \frac{c \bar{t}}{\lambda}, \\
M^2 &= \frac{\sigma B_0^2 a^2}{\mu_f}, \quad G_r = \frac{\rho_{nf} g \alpha a^2 \bar{T}_0}{c \mu_f}, \quad \xi = \frac{Q_0 a^2}{k_f \bar{T}_0},
\end{aligned} \tag{10}$$

in Eqs.(5-8), and using the assumptions of low Reynolds number and long wavelength, the non-dimensional governing conservation equations reduce to:

$$\frac{\partial p}{\partial r} = 0, \tag{11}$$

$$\frac{dp}{dz} = \frac{1}{(1-\phi)^{2.5}} \frac{1}{r} \frac{\partial}{\partial r} \left(r \frac{\partial w}{\partial r} \right) - M^2 (w+1) + G_r \theta, \tag{12}$$

$$0 = \frac{1}{r} \frac{\partial}{\partial r} \left(r \frac{\partial \theta}{\partial r} \right) + \xi \left(\frac{k_s + (m+1)k_f + \phi(k_f - k_s)}{k_s + (m+1)k_f - (m+1)(k_f - k_s)\phi} \right) = 0, \tag{13}$$

where M , ξ and G_r are the Hartmann number, heat absorption parameter and Grashof number respectively. In our analysis we consider a metachronal wave propagating along the walls of tube of mean radius (a) of the tube due to beating of cilia with the following dimensions: (ε) which designates the non-dimensional cilia length. Furthermore λ and c are the wavelength and wave speed of the metachronal wave, \bar{Z}_0 is the reference position of the particle and α is the measure of the eccentricity of the elliptical motion. The tube walls are sustained at constant temperature T_0 i.e. isothermal conditions, as shown in **Fig.1**. If the classical “no slip” boundary condition is applied on the inner tube wall, then the velocities of the transporting fluid are just those caused by the cilia tips, which can be given (see [17-31]) as:

$$\bar{W} = \left. \frac{\partial \bar{Z}}{\partial \bar{t}} \right|_{\bar{Z}_0} = \frac{\partial \bar{g}}{\partial \bar{t}} + \frac{\partial \bar{g}}{\partial \bar{Z}} \frac{\partial \bar{Z}}{\partial \bar{t}} = \frac{\partial \bar{g}}{\partial \bar{t}} + \frac{\partial \bar{g}}{\partial \bar{Z}} \bar{W}, \tag{14}$$

$$\bar{V} = \left. \frac{\partial \bar{R}}{\partial \bar{t}} \right|_{\bar{Z}_0} = \frac{\partial \bar{f}}{\partial \bar{t}} + \frac{\partial \bar{f}}{\partial \bar{Z}} \frac{\partial \bar{Z}}{\partial \bar{t}} = \frac{\partial \bar{f}}{\partial \bar{t}} + \frac{\partial \bar{f}}{\partial \bar{Z}} \bar{W}. \tag{15}$$

Eqns. (14) and (15) may also be expressed as:

$$\bar{W} = \frac{-\frac{2\pi}{\lambda}(\varepsilon\alpha ac \cos(\frac{2\pi}{\lambda})(\bar{Z} - c\bar{t}))}{1 - \frac{2\pi}{\lambda}(\varepsilon\alpha a \cos(\frac{2\pi}{\lambda})(\bar{Z} - c\bar{t}))}, \quad (16)$$

$$\bar{V} = \frac{\frac{2\pi}{\lambda}(\varepsilon ac \sin(\frac{2\pi}{\lambda})(\bar{Z} - c\bar{t}))}{1 - \frac{2\pi}{\lambda}(\varepsilon\alpha a \cos(\frac{2\pi}{\lambda})(\bar{Z} - c\bar{t}))}. \quad (17)$$

In the fixed coordinate system (\bar{R}, \bar{Z}) , flow within the tube is unsteady. It becomes steady in a wave frame (\bar{r}, \bar{z}) moving with the same speed as the wave moves in the \bar{Z} – direction. The transformations between the both frames are:

$$\bar{r} = \bar{R}, \quad \bar{z} = \bar{Z} - c\bar{t}, \quad \bar{v} = \bar{V}, \quad \bar{w} = \bar{W} - c, \quad \bar{p}(\bar{z}, \bar{r}, \bar{t}) = \bar{p}(\bar{Z}, \bar{R}, \bar{t}). \quad (18)$$

The boundary conditions induced by cilia movement are defined as:

$$\frac{\partial w}{\partial r} = 0, \quad \frac{\partial \theta}{\partial r} = 0 \quad \text{at } r = 0, \quad (19a)$$

$$w = \frac{-2\pi\varepsilon\alpha\beta \cos(2\pi z)}{1 - 2\pi\varepsilon\alpha\beta \cos(2\pi z)} - 1, \quad \theta = 0 \quad \text{at } r = h(z) = 1 + \varepsilon \cos(2\pi z). \quad (19b)$$

3. ANALYTICAL SOLUTIONS

Solving Eqns. (12 & 13) together with boundary conditions, Eqns.(19a & 19b), the *axial velocity* is obtained as:

$$w(r, z) = \frac{G_r \left(\frac{k_f}{k_{nf}} \right) \xi \left(M^2 T (h - r)(h + r) - 4 \right) + \frac{4I_0(Mr\sqrt{T}) \left(G \left(\frac{k_f}{k_{nf}} \right) \xi(s-1) + M^4(2s-1)T + M^2 \frac{dp}{dz}(s-1)T \right)}{(s-1)I_0(hM\sqrt{T})} - 4M^2 T \left(M^2 + \frac{dp}{dz} \right)}{4M^4 T}, \quad (20)$$

The *temperature field* emerges as:

$$\theta(r, z) = \frac{1}{4} \left(\left(\frac{k_s + (m+1)k_f + \phi(k_f - k_s)}{k_s + (m+1)k_f - (m+1)(k_f - k_s)\phi} \right) \right) (h^2 - r^2) \xi. \quad (21)$$

The *volumetric flow rate* is defined as:

$$F = 2 \int_0^{h(z)} r w dr. \quad (22)$$

Using Eqns. (20) & (22), the *axial pressure gradient* is obtained :

$$\frac{dp}{dz} = \frac{I_0(hM\sqrt{T})\left(G_r h^2\left(\frac{k_f}{k_{nf}}\right)\xi(h^2 M^2 T - 8) - 8M^4 T(F + h^2)\right) + \frac{8h^2 {}_0F_1\left(2; \frac{1}{4}h^2 M^2 T\right)\left(G_r\left(\frac{k_f}{k_{nf}}\right)\xi(s-1) + M^4(2s-1)T\right)}{s-1}}{h^4 M^4 T^2 {}_0F_1\left(3; \frac{1}{4}h^2 M^2 T\right)}, \quad (23)$$

where $T = (1 - \phi)^{2.5}$, $s = 2\pi\alpha\beta\varepsilon \cos(2\pi z)$.




The *pressure rise* is defined as:

$$\Delta P = \int_0^1 \frac{dp}{dz} dz. \quad (24)$$

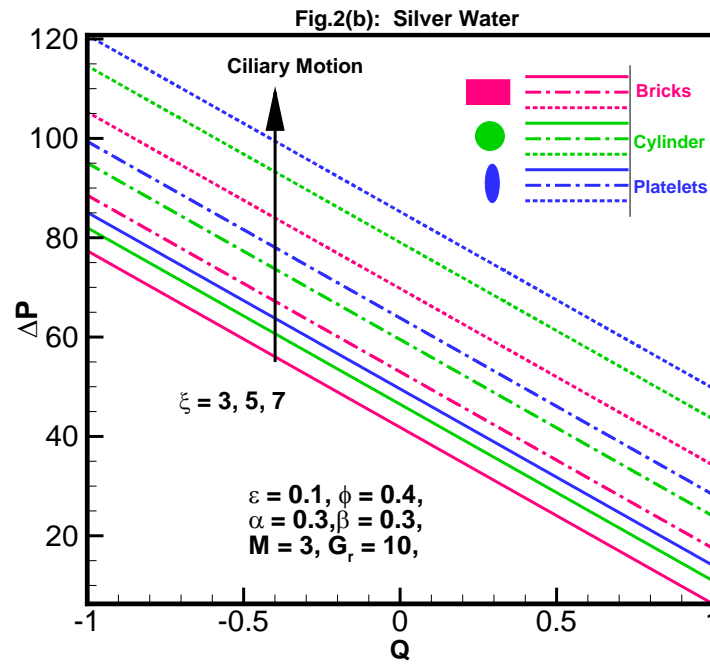
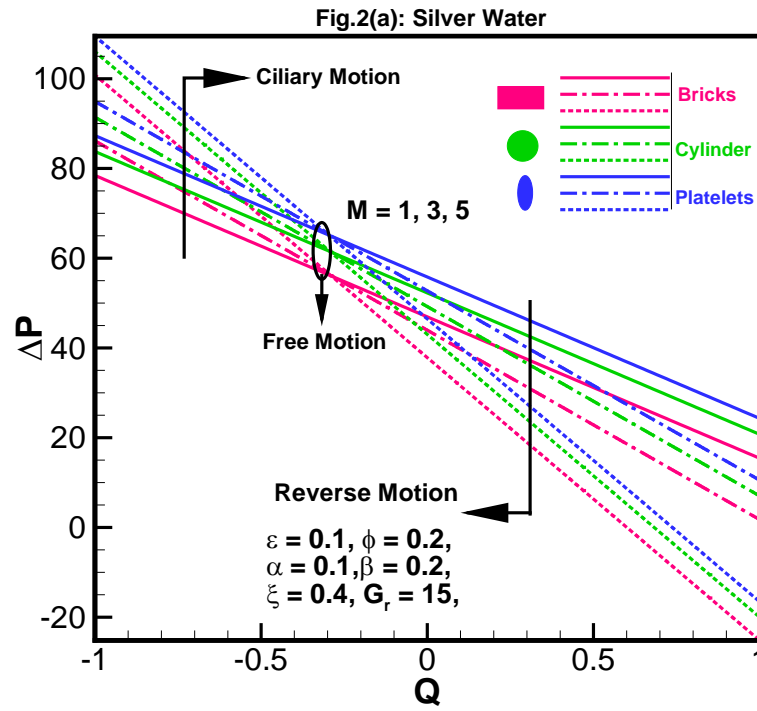
The *stream function* in the wave frame (obeying the Cauchy-Riemann equations, $u = \frac{1}{r} \frac{\partial \psi}{\partial r}$ and $v = -\frac{1}{r} \frac{\partial \psi}{\partial z}$) can be computed numerically with help of Eq.(20).

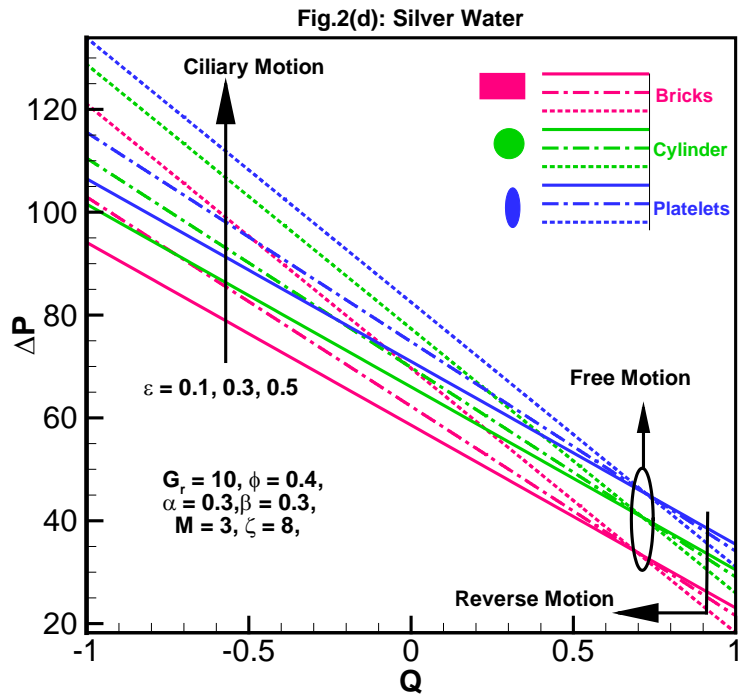
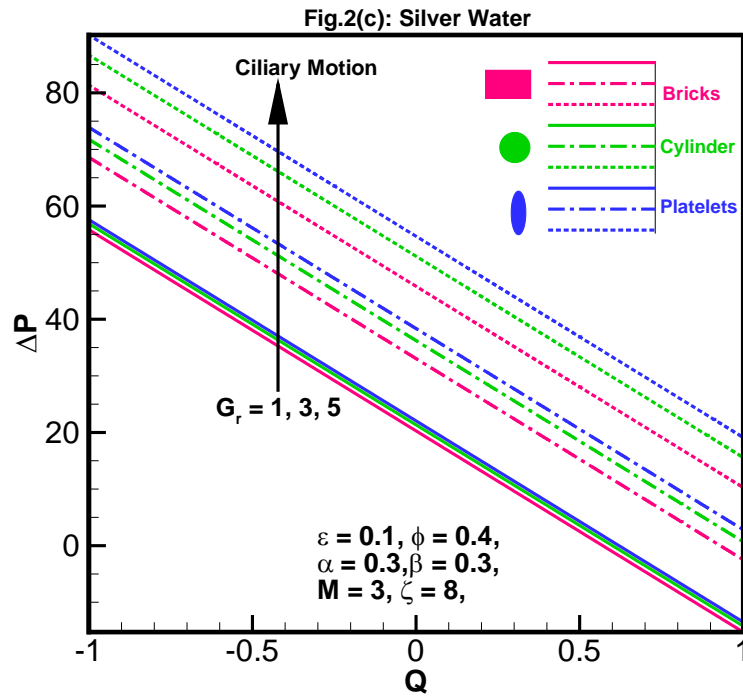
4. COMPUTATIONAL RESULTS AND DISCUSSION

Let us now consider the influence of key physical parameters emerging in the solutions defined in the previous section. This allows a parametric appraisal of the fundamental characteristics of magnetohydrodynamic convective heat transfer in creeping steady flow of silver nanofluid through the circular tube. We explore the effects of Hartmann number (M), heat absorption parameter (ξ), Grashof number (G_r) and amplitude ratio (ε) and nano-particle volume fraction (ϕ) on pressure rise, pressure gradient, thermal conductivity, temperature profile, velocity profile and trapping phenomenon via **Figs. (2-7)**. Thermophysical values of silver nanofluid are summarized in **Table 1** with respect to different nano-particle geometries. The anti-bacterial properties of silver-water nanofluid make it particularly appropriate for medical applications [35-37].

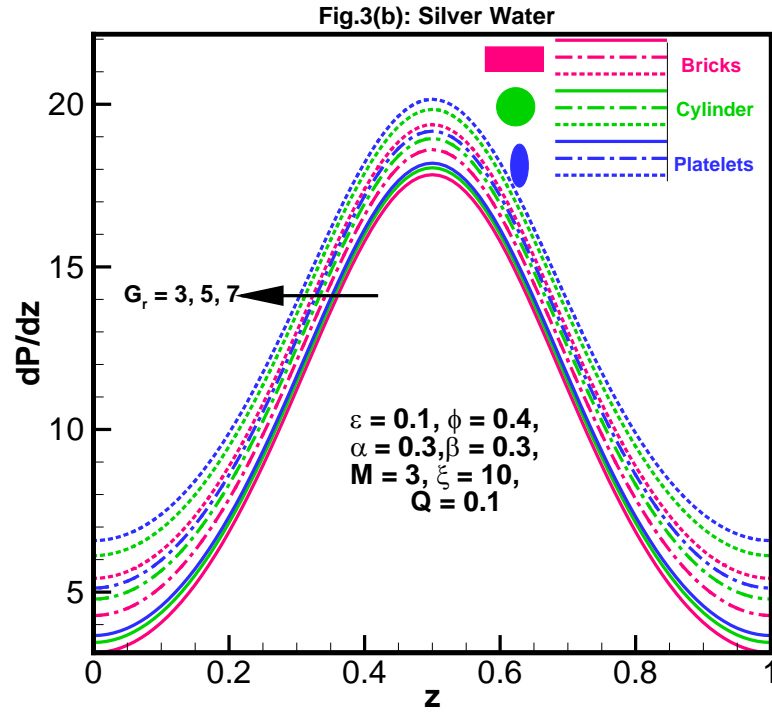
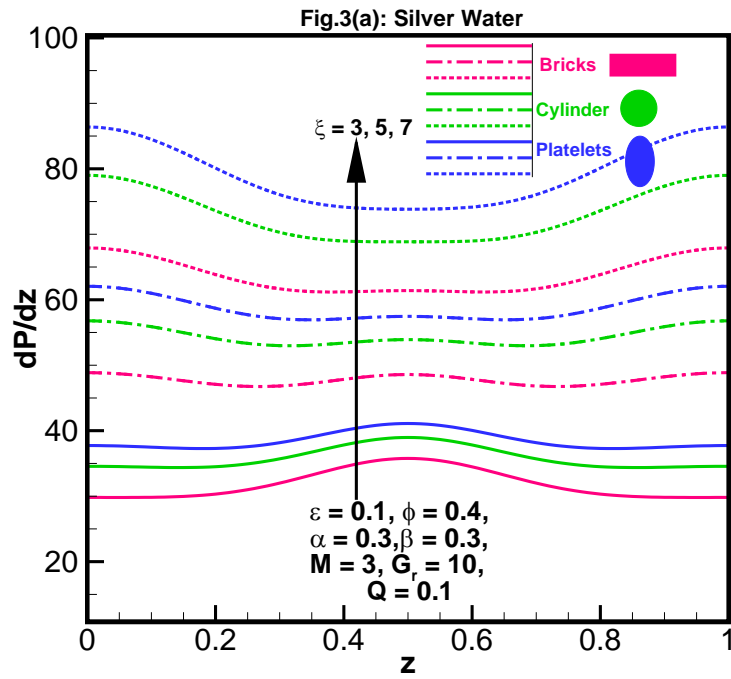
Table.1 Thermo physical properties of water and nanoparticles.					
Property	Water (H ₂ O)	Silver (Ag)	Particles Type	Shape	Shape factor m
ρ	997.1	10500	Bricks		3.7
c_p	4179	235	Cylinders		4.9
k	0.613	429	Platelets		5.7

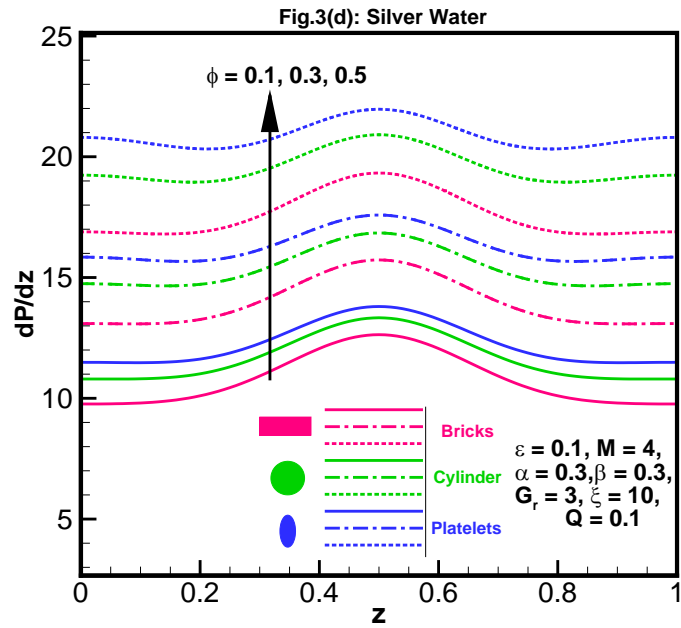
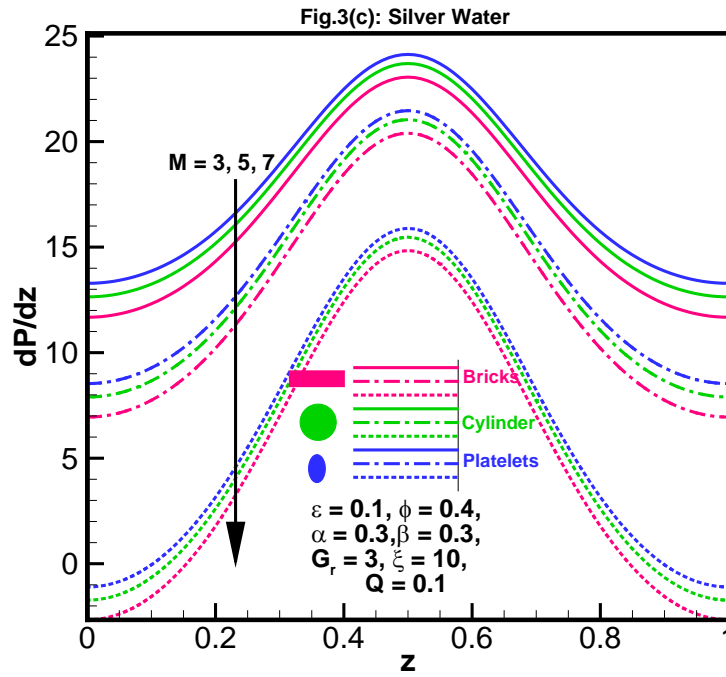
Figs.2 (a-d) depict the variation of pressure rise against the averaged flow rate under the influence of different flow parameters i.e. Hartmann number (M), heat absorption parameter (ξ), Grashof number (G_r) and amplitude ratio (ε). The relationship between pressure rise and flow rate is *linear*. Pressure is observed to be a maximum when averaged volumetric flow rate is a maximum. Fig. 2(a) shows that the pressure rise (ΔP) is elevated with increasing magnitude of Hartmann number i.e. with greater transverse magnetic field imposition, for the ciliary motion scenario. However the reverse trend is computed for the free motion and reverse motion scenarios. Magnetic body force is therefore assistive in ciliary propulsion but resistive in free or reverse motion. The patterns observed concur with the observations in earlier models [30, 31] and also demonstrate quite good correlation with the findings of Khaderi *et al.* [33] and Lin *et al.* [34], although these studies omitted heat transfer. The hydrodynamic trends nevertheless seem similar indicating that the correct behavior is computed based on the solutions developed in the present analysis.





Figs. 2. Variation of pressure rise (ΔP) against averaged flow rate (Q) for different nanoparticle shapes with various thermo-physical parameters: (a) M , (b) ξ , (c) G_r and (d) ε .





Figs. 3. Variation of axial pressure gradient (dP/dz) against axial coordinate (z) for different nanoparticle shapes with various thermo-physical parameters: (a) ξ , (b) G_r , (c) M and (d) ϕ .

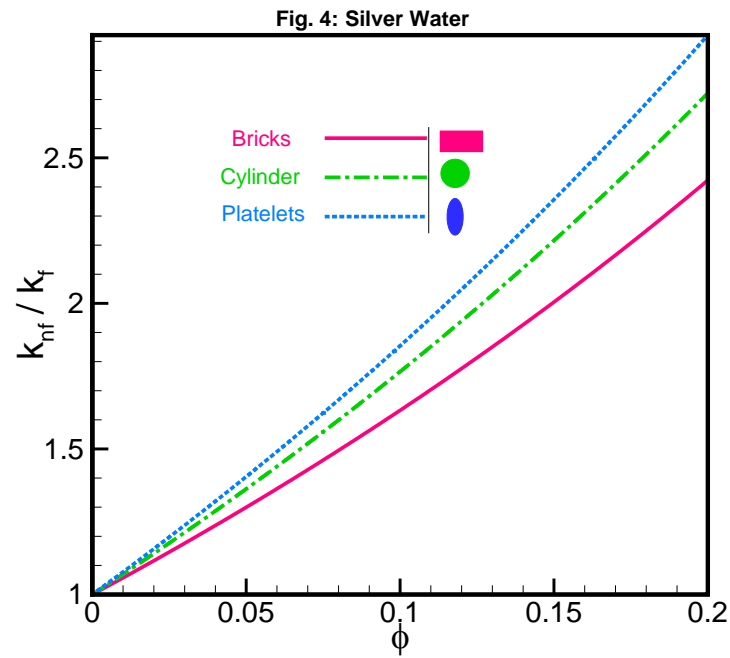
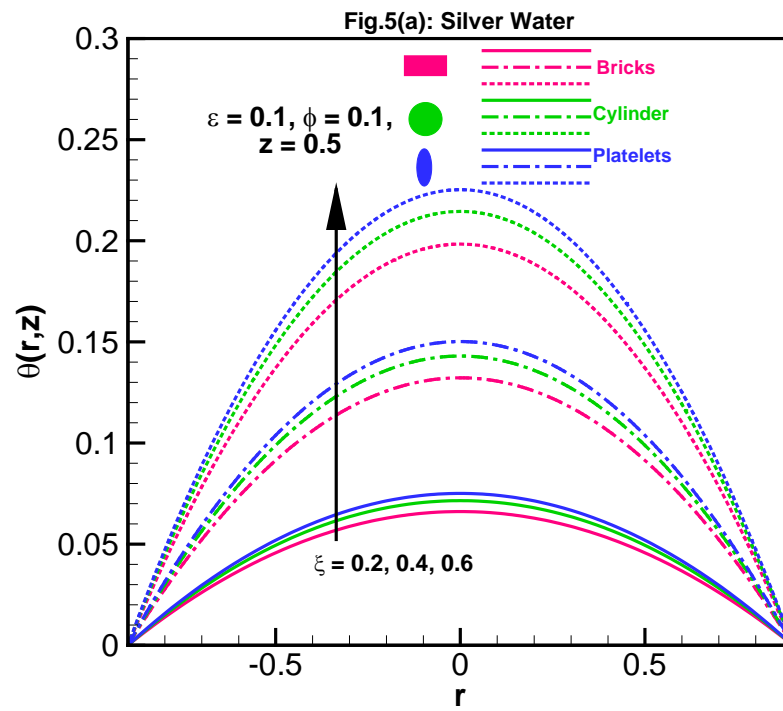
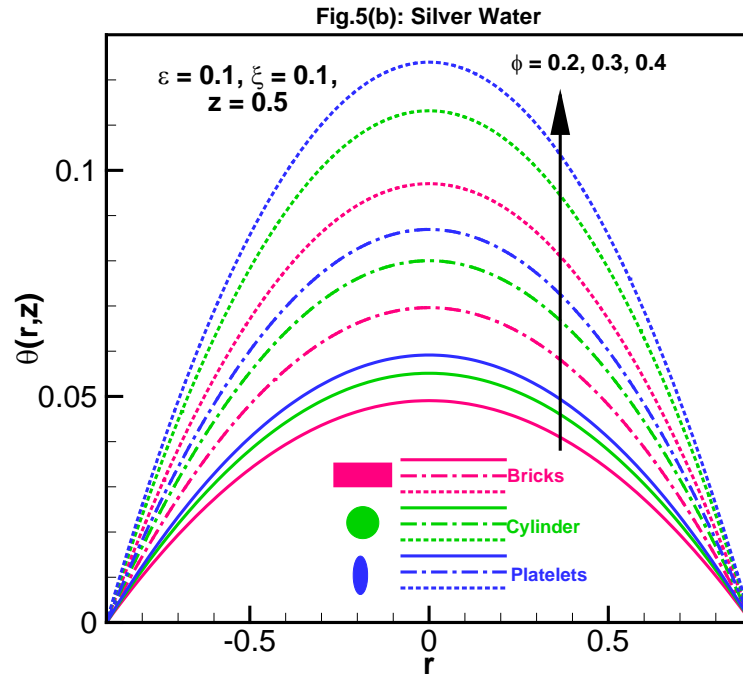
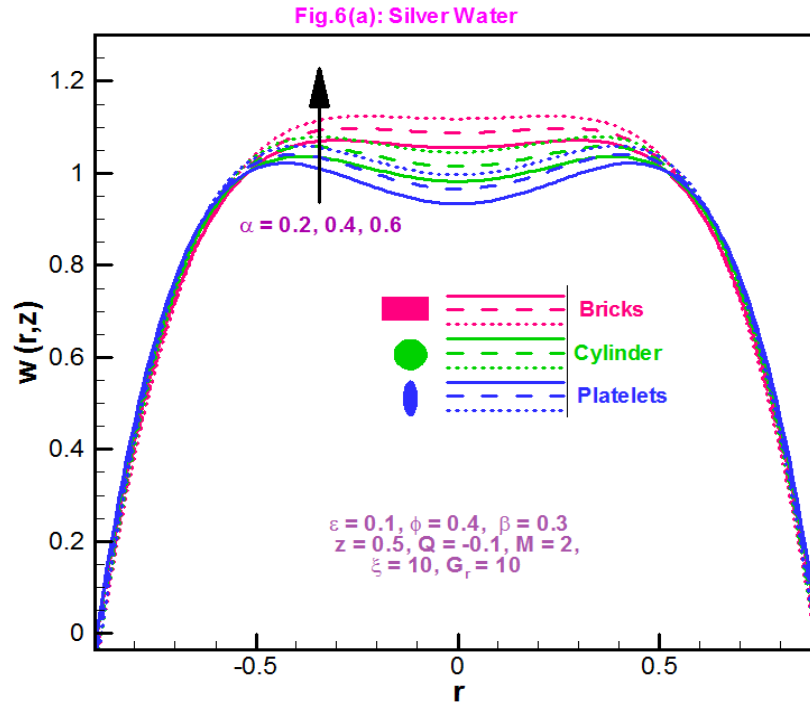


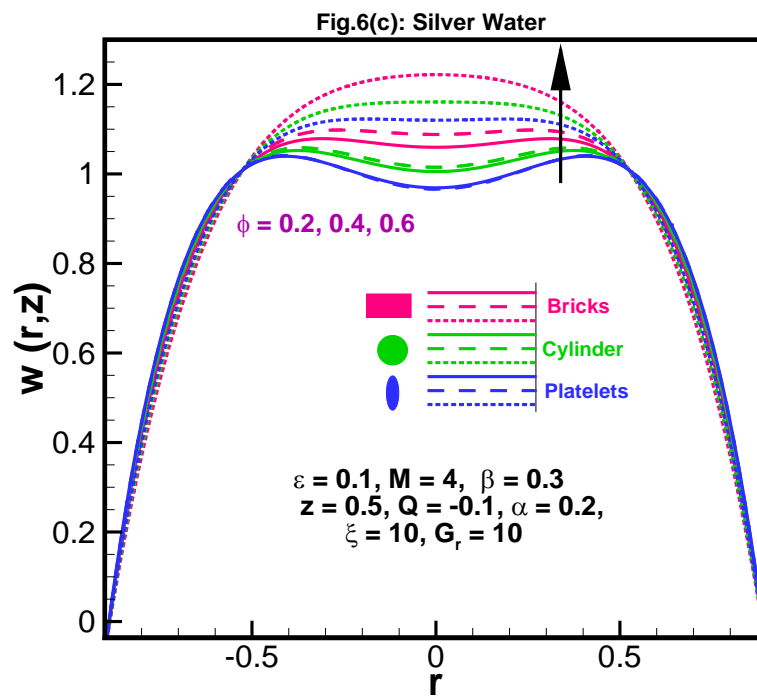
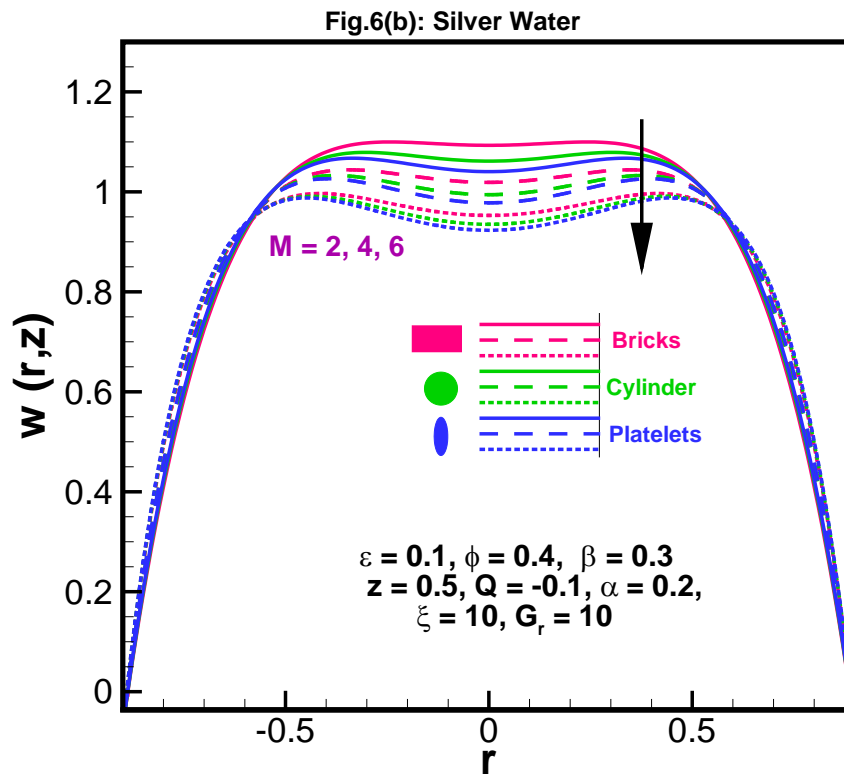
Fig. 4. Variation of effective thermal conductivity of the nanofluid (k_{nf}/k_f) with nano-particle volume fraction (ϕ) for different nanoparticle shapes.

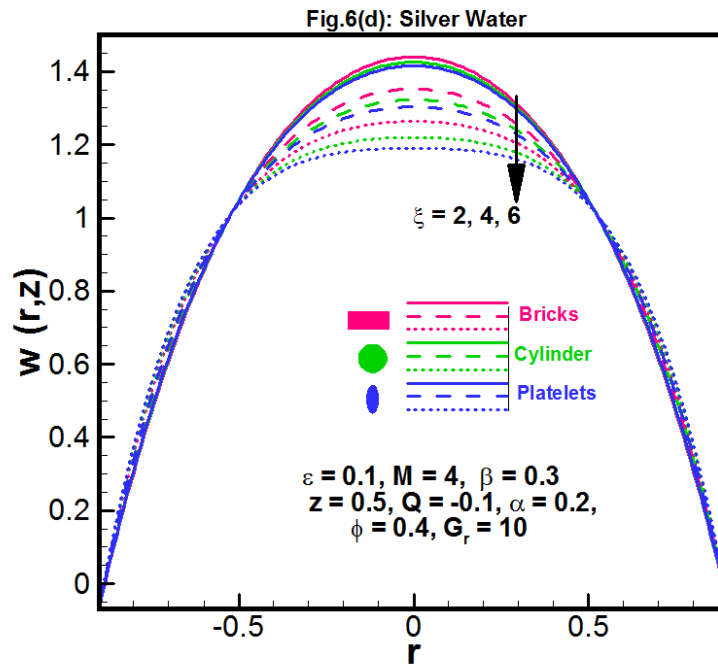




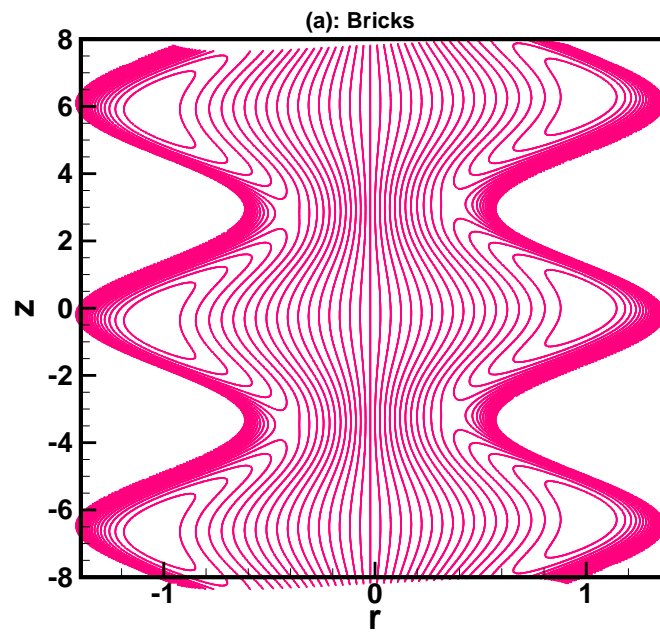
Figs. 5. Variation of temperature profile, $\theta(r, z)$ with radial coordinate (r) for different nanoparticle shapes with various thermo-physical parameters: (a) ξ , (b) ϕ .







Figs. 6. Axial velocity $w(r, z)$ vs. radial coordinate (r) for different nanoparticle shapes with various thermo-physical parameters: a) α , b) M , c) ϕ and d) ξ .



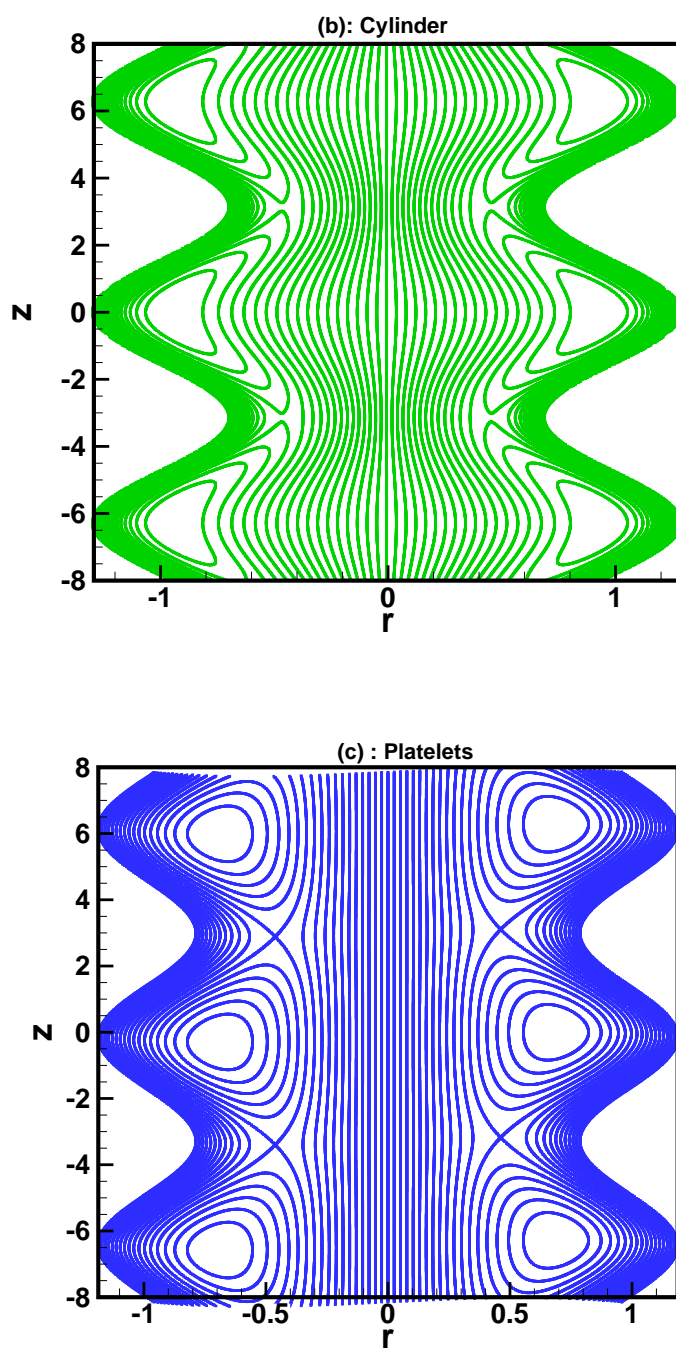


Fig.7. Streamline plots for different nanoparticle shapes.

Table. 2. Velocity profile for different nanoparticle shapes with fixed Hartmann number, $M=2$, and with $z = 0.25$, $Q = -0.1$, $G_r = 10$, $\varepsilon = 0.1$, $\beta = 0.3$, $\varphi = 0.1$, $\xi = 10$, $\alpha = 0.4$.

r	$w(r,z)$: Bricks	$w(r,z)$: Cylinders	$w(r,z)$: Platelets
-1.0	0.0000	0.0000	0.0000
-0.5	0.7587	0.7655	0.7385
0	0.5733	0.5107	0.5914
0.5	0.7587	0.7655	0.7385
1.0	0.0000	0.0000	0.0000

Table. 3. Temperature profile for different nanoparticle shapes with fixed heat source parameter, $\xi=0.2$, and with $z = 0.25$, $\varepsilon = 0.1$, $\varphi = 0.1$.

r	$\theta(r,z)$: Bricks	$\theta(r,z)$: Cylinders	$\theta(r,z)$: Platelets
-1.0	0.0000	0.0000	0.0000
-0.5	0.0229	0.0202	0.0212
0	0.0306	0.0269	0.0283
0.5	0.0229	0.0202	0.0212
1.0	0.0000	0.0000	0.0000

Table. 4. Pressure rise versus flow rate for different nanoparticle shapes with fixed Hartmann number, $M=5$, and with $\varepsilon = 0.1$, $\varphi = 0.4$, $G_r = 5$, $\beta = 0.2$, $\xi = 8$, $\alpha = 0.1$.

Q	ΔP : Bricks	ΔP : Cylinders	ΔP : Platelets
-1.0	100.8621	106.037	109.485
-0.5	69.3524	74.5289	77.9776
0	37.8446	43.0211	46.4697
0.5	6.33675	11.5132	14.9619
1.0	-25.1711	-19.9946	-16.546

Table. 5. Axial pressure gradient for different nanoparticle shapes with fixed Hartmann number, $M=0.5$, and with $Q = 0.1$, $\varepsilon = 0.1$, $\varphi = 0.4$, $G_r = 15$, $\beta = 0.3$, $\alpha = 0.3$, $\xi = 0.4$.			
z	dP/dz : Bricks	dP/dz : Cylinders	dP/dz : Platelets
0	12.1182	13.0816	13.7235
0.5	23.2964	23.9414	24.3712
1	12.1182	13.0816	13.7235

Fig. 2(b) shows that the pressure increases with increasing magnitude of heat absorption parameter i.e. heat intake into the flow increases pressure magnitudes. Fig. 2(c) indicates that pressure is elevated with magnitude of Grashof number. Therefore thermal buoyancy force is observed to enhance pressures in the regime. Similar observations have been made by Nadeem and Sadaf [31]. Free convection effects apparently therefore exert a considerable effect on the propulsion in ciliated thermal flow. Fig. 2(d) indicates that the pressure rise is a monotonic increasing function of amplitude ratio. A comparative study for different shaped nanoparticles on pressure rise is also computed through Figs. 2(a-d) and it is observed that pressure rise for platelets case is a maximum as compared to bricks and cylinder nanoparticles. The platelet nanoparticle shape therefore would appear to achieve the best pressure enhancement in ciliated magnetic bio-propulsion.

Figs. 3 (a-d) illustrate the influence of several key parameters on the *axial pressure gradient*. The profiles reveal that pressure gradient has a sinusoidal behavior along the axial direction. Fig. 3(a) demonstrates that pressure gradient rises with an increase in heat absorption parameter. The momentum equation (12) is coupled to the energy equation (13) via the thermal buoyancy term, $G_r\theta$. Thermal field therefore influences the momentum field considerably via the heat absorption term in eqn. (13) which also features nano-particle volume fraction, i.e. $\xi \left(\frac{k_s + (m+1)k_f + \phi(k_f - k_s)}{k_s + (m+1)k_f - (m+1)(k_f - k_s)\phi} \right)$. Figs. 3(b & c) show clearly the monotonic increasing behavior with Grashof number (the ratio of buoyancy forces to viscous forces) and nanoparticle

fraction (ϕ). Fig.3 (d) shows the effect of Hartmann number (magnetic field parameter) on pressure gradient. A significant reduction in pressure gradient is observed with increasing Hartmann number (ratio of electromagnetic forces to viscous force increases). The increase in magnetic drag force relative to viscous force evidently inhibits flow. It is further noticed that pressure gradient is greater for platelet nanoparticles as compared with brick and cylindrical nanoparticle geometries.

Fig. (4). presents the variation in the effective thermal conductivity of silver-water nanofluid for different shape of the nanoparticles i.e. bricks, cylinder and platelets. Inspection of the figure shows that a substantial difference is computed in the thermal conductivities for different nanoparticle geometries, with *platelet nanoparticles* evidently exhibiting the maximum thermal conductivity values and brick nanoparticles achieving the lowest effective thermal conductivity values. It has been experimentally observed (see Choi [2] and Das *et al.* [3]) that solid nanoparticle volume fraction is *directly proportional* to the thermal conductivity of the fluid. This observation is consistent with the present computations since it is evident from Fig.4 that the higher the solid nanoparticle fraction, the greater the thermal conductivity of the fluid.

Figs. 5(a-b) illustrate the collective influence of *different nanoparticle shapes, heat absorption parameter and nanoparticle fraction* on the temperature distribution in the vertical tube. Temperature of the nanofluid is clearly greater at the center of the tube and significantly less at the walls of the tube. This observation is consistent with other investigations [31]. It is also apparent that temperature *rises* as we change the shape of nanoparticles from bricks to cylinders and platelets respectively. Fig. 5(a) indicates that temperature significantly increases with an increase in the heat absorption parameter which is physically logical since thermal energy is being introduced into the propulsive flow. Many other classical studies of heat transfer have confirmed this trend and the reader is referred to Gebhart *et al.* [38] and also Tien *et al.* [39] [39]. Fig. 5(b) shows also that increasing nanoparticle fraction markedly elevates temperature which confirms the thermal-enhancing properties of nanofluids [2]. This further implies that in medical ciliated propulsion systems, nanoparticles can elevate thermal performance considerably and this may be of potential benefit in disease treatment where heat enhancement properties may assist in the delivery of drugs.

Figs.6(a)-6(d) present the velocity profile evolution (axial velocity vs radial coordinate)

for different nanoparticle shapes i.e. bricks, cylinder and platelets and also for different values of the measure of the eccentricity of the elliptical motion (α), Hartmann number (M), nanoparticle fraction (ϕ) and heat absorption parameter (ξ). It is observed that when eccentricity measure of the elliptical motion (α) is increased and also with greater nanoparticle fraction (ϕ), velocity profile is somewhat reduced near the tube wall while it is increased in the core region of the tube. Evidently therefore the primary acceleration is in the central zone of the tube. When the magnitudes of Hartmann number and heat absorption parameter are increased, velocity profile conversely is increased near the tube wall whereas it is depressed at the center of the tube. Increasing hydromagnetic body force therefore, as expected, decelerates the core flow whereas it accelerates the near-wall flow, and this behavior has been reported in many studies, both of conventional magnetic fluids (see Cramer and Pai [40]) and also nanofluids (see Akbar *et al.* [12]). Furthermore these trends corroborate other studies of magnetic nanofluid transport including Hayat *et al.* [41, 42], Malvandi *et al.* [43] and Servati *et al.* [44] which also demonstrate that the dominant influence of an external magnetic field is to significantly modify velocity profiles. Indeed the authors have also observed similar patterns of influence in other recent works concerning electromagnetic nanofluid transport phenomena [45, 46]”

It is also evident that velocity magnitudes are lower for platelet nanoparticles whereas they are enhanced bricks nanoparticles.

Figs. 7(a-c) present streamline distributions for different nanoparticle shapes (bricks, cylinder and platelets) and these are obtained by taking the value of stream function as zero. The trapping of streamlines is a characteristic phenomenon associated with physiological propulsion in deformable vessels. By visualizing center stream lines as circulated/closed for appropriate combinations of the values of amplitude and averaged flow rate, it is possible then to examine bolus formation dynamics. The plots demonstrate that the number of trapped streamlines for cylinder type nanoparticles is greater as compared with brick and platelet nanoparticles, whereas the size of the bolus (trapped zones) for brick nanoparticles is markedly larger relative to cylinder and platelet nanoparticles.

In **Tables 2-3** further solutions have also been provided for the velocity, temperature, pressure rise and axial pressure gradient variation with various parameters for each nanoparticle shape i.e. brick, platelet and cylinder silver (Ag) nanoparticles in water. **Table 2** shows that axial velocity

is generally maximum in the core region (low radial coordinate) with fixed Hartmann number ($M=2$ indicating that magnetic body force is double the viscous hydrodynamic force) and are a maximum for brick nano-particles whereas they are a minimum for cylindrical nanoparticles in the core region of the tube. **Table 3** shows highest temperatures are associated with the brick nano-particles in the core region of the tube whereas the lowest temperatures are computed for cylindrical nano-particles. **Table 4** indicates that with increasing positive flow rate ($Q>0$), there is a significant decrease in pressure rise for all nano-particle scenarios. However platelet nanoparticles generally achieve the highest value of pressure rise whereas brick nano-particles produce the lowest magnitudes of pressure rise. **Table 5** shows that platelet nano-particles attain the highest axial pressure gradient through the tube, whereas brick nano-particles achieve the lowest values for pressure gradient. We further note that detailed elucidation of *why certain shapes have certain influence* requires a more complex surface analysis of the problem. This could be explored via molecular dynamics simulations where topology can be very precisely simulated rather than via a shape factor, although this is not the focus of the present work. It is envisaged that readers may wish to further explore this pathway in the future.

5. CONCLUSIONS

A mathematical model has been developed to simulate magnetohydrodynamic convective heat transfer in nanofluid flow through a vertical tube induced by metachronal wave propagation under a uniform radial magnetic field. Under creeping flow approximations, and using an elliptical model for the cilia beating, the conservation equations for mass, momentum and energy are transformed from a moving to a stationary frame of reference and solved analytically under appropriate boundary conditions. Three different nanoparticle geometries (i.e. bricks, platelets and cylinders) are addressed. Closed-form expressions are derived for the effective thermal conductivity of nanofluid, axial velocity, temperature, axial pressure gradient and mean volumetric flow rate. The influence of cilia length parameter, Hartmann (magnetic) number, heat absorption parameter, Grashof number (free convection), solid nanoparticle volume fraction, and cilia eccentricity parameter on the flow and heat transfer characteristics (including effective thermal conductivity of the nanofluid) have been examined in detail. On the basis of numerical

results derived, some significant findings of the present investigation are summarized below:

- Pressure rise is a monotonical increasing function of the Hartmann (magnetic) number, heat absorption, Grashof number and amplitude ratio parameter.
- The thermal conductivity for platelets nanoparticles is greater than for brick or cylindrical nanoparticles.
- The temperature is significantly elevated with increasing magnitude of heat absorption parameter and also with nanoparticle fraction.
- Temperature is also strongly dependent on the geometry of nanoparticles and progressively higher values are computed for bricks, cylinders and platelet nano-particles i.e. the platelet nano-particles attain highest temperatures.
- Velocity magnitudes are reduced with increasing measure of the eccentricity of the metachronal wave and also with nanoparticle fraction near the tube wall whereas the opposite trend is computed at the central (core) region of the tube.
- Velocity magnitude is elevated with greater values of Hartmann number and heat absorption parameter *near the tube wall* with the converse pattern computed *in the central (core) region* of the tube.
- More streamlines are trapped for cylindrical nanoparticles as compared with brick or platelet nanoparticles.

REFERENCES

- [1] A. Bilgin *et al.*, Magnetic nanoparticle based nanofluid actuation with dynamic magnetic fields. In: *Proc. ASME 2011 9th Int. Conference on nanochannels, microchannels, and minichannels, ICNMM 9, June 19–22, Edmonton, Canada, ICNMM2011-58222*, 2011.
- [2] S. U.S. Choi, Enhancing thermal conductivity of fluids with nanoparticles, in *Developments and Applications of Non-Newtonian Flows*, eds. D. A. Singer and H. P. Wang, vol. FED 231, pp. 99–105, American Society of Mechanical Engineers, New York, 1995.
- [3] S. K. Das, S. U. S. Choi, H. E. Patel, Heat transfer in nanofluids- a review, *Heat Transfer Engineering*, 27(10):3–19, 2006.
- [4] D. Wen, G. Lin, S. Vafaei, K. Zhang, Review of nanofluids for heat transfer applications,

Particuology 7 (2009) 141–150.

[5] V. Trisaksri, S. Wongwises, Critical review of heat transfer characteristics of nanofluids, *Renewable and Sustainable Energy Reviews*, 11 (2007) 512–523

[6] Q. Wang, Arun S. Mujumdar, Heat transfer characteristics of nanofluids: a review, *Int. J. Thermal Sciences*, 46 (2007) 1–19.

[7] M.J. Uddin, P. Rana, O. Anwar Bég and A. I. Md. Ismail, Finite element simulation of magnetohydrodynamic convective nanofluid slip flow in porous media with nonlinear radiation, *Alex. Eng. J* (2016). 15 pages. doi:10.1016/j.aej.2016.04.021

[8] M. Sheikholeslami, Mofid Gorji Bandpy, R. Ellahi, A. Zeeshan, Simulation of MHD CuO–water nanofluid flow and convective heat transfer considering Lorentz forces, *J. Magnetism and Magnetic Materials*, 369 (2014) 69–80.

[9] T. A. Bég, O. Anwar Bég, M. M. Rashidi and M. Asadi, Homotopy semi-numerical modelling of nanofluid convection flow from an isothermal spherical body in a permeable regime, *Int. Journal of Microscale and Nanoscale Thermal and Fluid Transport Phenomena*, 3, 67-96 (2012).

[10] O.D. Makinde, W.A. Khan, Z.H. Khan, Buoyancy effects on MHD stagnation point flow and heat transfer of a nanofluid past a convectively heated stretching/shrinking sheet, *Int. J. Heat and Mass Transfer* 62 (2013) 526–533.

[11] M. Turkyilmazoglu, Exact analytical solutions for heat and mass transfer of MHD slip flow in nanofluids, *Chemical Engineering Science*, 84 (2012) 182–187.

[12] N. S. Akbar, D. Tripathi and O. Anwar Bég, Modelling nanoparticle geometry effects on peristaltic pumping of medical magnetohydrodynamic nanofluids with heat transfer, *J. Mechanics in Medicine and Biology*, 16 (2) 1650088.1-1650088.20. DOI: 10.1142/S0219519416500883 (2015). 20 pages

[13] O. Anwar Bég, M. Ferdows, Shamima Islam and M. Nazrul Islam, Numerical simulation of Marangoni magnetohydrodynamic bio-nanofluid convection from a non-isothermal surface with magnetic induction effects: a bio-nanomaterial manufacturing transport model, *J. Mechanics Medicine Biology*, 14, 3, 1450039.1-1450039.32 (32 pages) (2014). DOI: 10.1142/S0219519414500390

- [14] G. Fullstone, J. Wood, M. Holcombe & G. Battaglia, Modelling the transport of nanoparticles under blood flow using an agent-based approach, *Nature Scientific Reports*, 5:10649. DOI: 10.1038/srep10649 (2015).
- [15] M. Khan and W.A. Khan, MHD boundary layer flow of a power-law nanofluid with new mass flux condition, *AIP Advances*, 6, 25211 (2016). <http://dx.doi.org/10.1063/1.4942201>
- [16] Y. Bao *et al*, Magnetic nanoparticles: material engineering and emerging applications in lithography and biomedicine, *J. Materials Science*, 51, 513-553 (2016).
- [17] M. A. Sleight. *The Biology of Cilia and Flagella*, MacMillan, New York, USA (1962).
- [18] M. A. Sleight and E. Aiello, The movement of water by cilia, *Acta. Protozool.*, 11, 265-277 (1972).
- [19] C. E. Miller, An investigation of the movement of Newtonian liquids initiated and sustained by the oscillation of mechanical cilia, *Aspen Emphysema Conf.* 10 (1967) 309–321.
- [20] J. R. Blake, A spherical envelope approach to ciliary propulsion, *J. Fluid Mechanics*, 46, 199-208 (1971).
- [21] J. R. Blake, Flow in tubules due to ciliary activity, *Bull Math Biol.*, 35, 513-523 (1973).
- [22] S. N. Khaderi *et al.*, Magnetically-actuated artificial cilia for microfluidic propulsion, *Lab Chip*, 11, 2002 (2011).
- [23] A. Dauplain, J. Favier and A. Battaro, Hydrodynamics of ciliary propulsion, *J. Fluids Struct.* 24, 1156–1165 (2008).
- [24] S. N. Khaderi, J. M. J. den Toonder and P. R. Onck, Fluid flow due to collective non-reciprocal motion of symmetrically-beating artificial cilia, *Biomicrofluidics*, 6, 014106 (2012).
- [25] S. N. Khaderi and P. R. Onck, Fluid--structure interaction of three dimensional magnetic artificial cilia, *J. Fluid Mechanics*, 708, 303-328 (2012).
- [26] F. Kotsis, Christopher Boehlke, and E. Wolfgang Kuehn, The ciliary flow sensor and polycystic kidney disease, *Nephrol. Dial Transplant* 28, 518–526 (2013).
- [27] J. M. Brown and G. B. Witman, Cilia and Diseases, *BioScience*, 64, 1126–1137 (2014).
- [28] N. S. Akbar, A. W. Butt, Heat transfer analysis of viscoelastic fluid flow due to metachronal wave of cilia, *Int. J. Biomathematics*, 7, 1450066 (2014). (14 pages)
- [29] N. S. Akbar, Z.H. Khan, Metachronal beating of cilia under the influence of Casson fluid and magnetic field, *J. Magnetism and Magnetic Materials*, 378, 320-326 (2015).

- [30] N. S. Akbar, Z. H. Khan, Heat transfer analysis of bi-viscous ciliary motion fluid, *Int. J. Biomathematics*, (8)(2015)1550026(13 pages).
- [31] S. Nadeem and H. Sadaf, Theoretical analysis of Cu-blood nanofluid for metachronal wave of cilia motion in a curved channel. *IEEE Trans. Nanobiosciences*, 14(2015)447-454.
- [32] J.V.I. Timonen *et al.*, A facile template-free approach to magnetodriven, multifunctional artificial cilia. *ACS Applied Materials and Interfaces*, 2, 22262230 (2010).
- [33] S.N. Khaderi *et al.*, Nature-inspired microfluidic propulsion using magnetic actuation. *Physical Review E* 79, 046304 (2009).
- [34] C.Y. Lin *et al.*, Fluid dynamics analysis of magnetically actuated ciliated nano/micro structures for flow mixing and propulsion applications, 8th *IEEE Nano/Micro Engineered and Molecular Systems (NEMS)*, Suzhou, China, April 7-10 (2013).
- [A] Hamilton, R. L., & Crosser, O. K. (1962). Thermal conductivity of heterogeneous two-component systems. *Industrial & Engineering Chemistry Fundamentals*, 1(3), 187-191.
- [B] Timofeeva, E. V., Routbort, J. L., & Singh, D. (2009). Particle shape effects on thermophysical properties of alumina nanofluids, *Journal of Applied Physics*, 106(1), 014304.
- [35] D. Maity *et al.*, In situ synthesis, characterization, and antimicrobial activity of silver nanoparticles using water soluble polymer, *J. Appl. Polymer Sci.*, 122, 2189–2196 (2011).
- [36] R.G. Fuentes *et al.*, Study of thermal diffusivity of nanofluids with bimetallic nanoparticles with Au(core)/Ag(shell) structure, *Appl. Surf. Sci.*, 255, 781–783 (2008).
- [37] J.L. Gardea-Torresdey *et al.*, Alfalfa sprouts: a natural source for the synthesis of silver nanoparticles. *Langmuir* 19:1357–1361 (2003).
- [38] B. Gebhart *et al.*, *Buoyancy-induced Flows and Transport*, Hemisphere, Washington, USA (1988).
- [39] C.L. Tien, A. Majumdar and F.M. Gerner (Editors), *Microscale Energy Transport*, 385 pp., Taylor & Francis, Washington, DC (1998).
- [40] K.C. Cramer and S. Pai, *Magnetofluid Dynamics for Engineers and Applied Physicists*, MacGraw-Hill, New York (1973).
- [41] Tasawar Hayat, Maria Imtiaz, Ahmed Alsaedi, Melting heat transfer in the MHD flow of Cu–water nanofluid with viscous dissipation and Joule heating, *Advanced Powder Technology*,

27, 1301-1308 (2016).

[42] T. Hayat, Taseer Muhammad, S.A. Shehzad, A. Alsaedi, On three-dimensional boundary layer flow of Sisko nanofluid with magnetic field effects, *Advanced Powder Technology*, 27, 504-512 (2016).

[43] A. Malvandi, S.A. Moshizi, D.D. Ganji, Effect of magnetic fields on heat convection inside a concentric annulus filled with Al_2O_3 -water nanofluid, *Advanced Powder Technology*, 25, 1817-1824 (2014).

[44] Ata A. Servati V., Koroush Javaherdeh, Hamid Reza Ashorynejad, Magnetic field effects on force convection flow of a nanofluid in a channel partially filled with porous media using Lattice Boltzmann Method, *Advanced Powder Technology*, 25, 666-675 (2014).

[45] Akbar, N. S., Tripathi, D., Khan, Z. H., and Bég, O. Anwar, A numerical study of magnetohydrodynamic transport of nanofluids over a vertical stretching sheet with exponential temperature-dependent viscosity and buoyancy effects. *Chemical Physics Letters*, 661, 20-30 (2016).

[46] Akbar, N. S., Tripathi, D., Bég, O. A., & Khan, Z. H. MHD dissipative flow and heat transfer of Casson fluids due to metachronal wave propulsion of beating cilia with thermal and velocity slip effects under an oblique magnetic field. *Acta Astronautica*, 128, 1-12 (2016).